ACS APPLIED MATERIALS & INTERFACES

Research Article

www.acsami.org

Double-Shell Architectures of $ZnFe_2O_4$ Nanosheets on ZnO Hollow Spheres for High-Performance Gas Sensors

Xiaowei Li, Chen Wang, Hang Guo, Peng Sun,* Fengmin Liu, Xishuang Liang, and Geyu Lu*

State Key Laboratory on Integrated Optoelectronics, College of Electronic Science and Engineering, Jilin University, Changchun 130012, People's Republic of China

Supporting Information

ABSTRACT: In this study, double-shell composites consisting of inner ZnO hollow microspheres (ZHS) surrounded by outer $ZnFe_2O_4$ nanosheets were successfully synthesized. The growth of the ultrathin $ZnFe_2O_4$ nanosheets (~10 nm) on the ZHS outer surface was carried out at room temperature via solution reactions in order to generate a double-shell configuration that could provide a large surface area. As a proof-of-concept demonstration of the design, a comparative sensing investigation between the sensors based on the as-obtained ZnO/$ZnFe_2O_4$ composites and its two individual components (ZnO hollow spheres and $ZnFe_2O_4$ nanosheets) was performed. As expected, the response of the $ZnFe_2O_4$-decorated ZnO composites to 100 ppm acetone was about 3 times higher than that of initial ZnO microspheres. Moreover, a dramatic reduction of response/recover time has been achieved at different operating temperature. Such favorable sensing performances endow these ZnO/$ZnFe_2O_4$ heterostructures with a potential application in gas sensing.

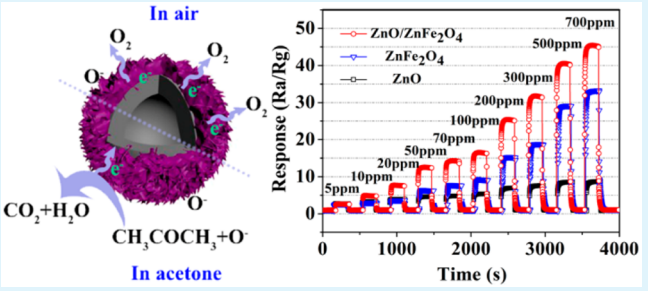

KEYWORDS: *ZnO/$ZnFe_2O_4$, double-shell, heterostructure, gas sensor, acetone*

1. INTRODUCTION

Oxide semiconductors, as promising candidates for gas-sensing materials, have been paid tremendous attention owing to their unique features like high sensitivity, low cost, controllable preparation, and facile integration.[1,2] Over the past few decades, numerous metal oxide semiconductors (MOS) have been developed for gas sensing. According to their majority charge carrier, these oxide semiconductors were broadly divided into n-type MOS (such as In_2O_3, SnO_2, ZnO, Fe_2O_3, WO_3, etc.)[3−6] and p-type MOS (such as NiO, Co_3O_4, and CuO).[7−10] Although much progress has been made, these pure single-component MOS still suffer from some drawbacks arising from their limited physical or chemical characters, which will hinder their further application in high-performance gas sensors. In virtue of their tunable chemical composition and synergistic properties, heterostructured composites are expected to exhibit much more excellent sensing performance. In this case, expanding the sensing materials from single-component MOS to multicomponent heterostructure has become more and more fascinating. Thus, the main focus of current studies is directed toward constructing heterostructures with different components. Up to now, various hybrid composites, such as ZnO/SnO_2,[11] Co_3O_4/TiO_2,[12] NiO/WO_3,[13] SnO_2/α-Fe_2O_3,[14] and CuO/ZnO,[15] have been obtained, and a series of inspiring properties that derived from the heterojunction between the individual components have been observed. The constant need for gas sensors with high sensitivity, fast response/recovery speed, low operating temperature, and good stability continues to stimulate the progress of gas sensing. Therefore, to achieve these desired performances of gas sensor, it is very important to make efforts in the rational design and synthesis of novel gas-sensing materials.

ZnO, a well-known n-type semiconductor material, has been well studied and applied in detection of many toxic gases including CO,[16] NH_3,[17,18] NOx,[19−21] and volatile organic compounds (VOC) gases.[22−24] Unfortunately, in spite of its multifunctional applications in the field of gas sensor, the broad sensitive characteristics make ZnO lose the selectivity to a certain gas. Therefore, improving the selectivity of oxide semiconductor remains a great challenge. Recently, various ternary oxide semiconductors with spinel structure, such as ferrites (MFe_2O_4, M = Cu, Mg, Zn, Ni, Cd), have stimulated great interest because of their excellent performance in many fields, such as gas sensors,[25,26] magnetic materials,[27,28] photocatalysis,[29,30] Li-ion batteries,[31−33] and photoelectrodes.[34] Among these ternary oxides, zinc ferrite ($ZnFe_2O_4$) has been demonstrated to be a promising candidate for gas sensing due to its excellent selectivity and/or high response to a specific target gas.[35,36] Considering the fact that enhanced performances of gas sensor usually can be achieved by combining the single-component oxides together, it is reasonable to expect that decorating the surface of ZnO with $ZnFe_2O_4$ would be an

Received: May 13, 2015
Accepted: July 28, 2015
Published: July 28, 2015

DOI: 10.1021/acsami.5b04118
ACS Appl. Mater. Interfaces 2015, 7, 17811−17818

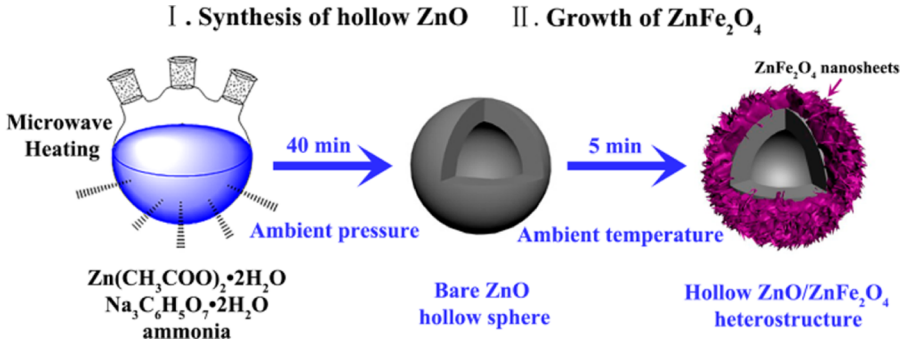

Figure 1. Schematic illustration of the formation of ZnO/$ZnFe_2O_4$ heterostructure using a facile two-step method.

efficient way to enhance the properties of pure ZnO. Recently, various strategies have been explored to synthesize the heterostructures, and some of them have been demonstrated to be reproducible.[37−39] However, some serious disadvantages, such as sophisticated synthetic procedures, long reaction time, and rigid environmental conditions, are hindering their further practical application. Therefore, developing a more facile strategy for preparing heterostructures is still a fundamental issue in materials science.

In this current work, ZnO/$ZnFe_2O_4$ double-shell structures have been synthesized using a mild method which involves the microwave-assisted synthesis of ZnO hollow microspheres and the subsequent decoration with homogeneous $ZnFe_2O_4$ nanosheets. It is worth mentioning that these ultrathin $ZnFe_2O_4$ nanosheets can be easily decorated on the surface of ZnO by simply stirring at ambient temperature (25 °C). Moreover, for the convenience of comparison, the gas-sensing performances of ZnO/$ZnFe_2O_4$ composites, pristine ZnO microspheres, and pure $ZnFe_2O_4$ nanosheets were all investigated. As expected, the results reveal that the sensor based on as-prepared ZnO/$ZnFe_2O_4$ exhibited much more excellent sensing properties in terms of sensitivity, selectivity, operating temperature, and response/recover speed.

2. EXPERIMENTAL PROCEDURE

All of the chemical reagents involved in this experiment were purchased from Beijing Chemicals Co. Ltd. of China and directly used as received without further purification. The designed experimental procedure is schematically illustrated in Figure 1.

2.1. Synthesis of Material. *Synthesis of ZnO Hollow Microspheres.* The ZnO hollow microspheres were first synthesized according to our previous work with some modification.[23] In a typical process, 200 mL of aqueous solution containing 5 mmol of zinc acetate dihydrate ($Zn(CH_3COO)_2·2H_2O$) and 0.2 mmol of trisodium citrate dihydrate ($Na_3C_6H_5O_7·2H_2O$) was first prepared at room temperature. Then, 6 mL of ammonia (30 wt % NH_3 in water) was added into the above solution. After thorough mixing, the resulting transparent solution was transferred into a three-necked flask and maintained at 90 °C for 40 min with the assistance of microwave heating (300 W, MAS-II, Shanghai Xinyi Ltd.). After the reaction, the white products were collected and washed by centrifugation several times before being vacuum-dried at 60 °C.

Synthesis of ZnO@$ZnFe_2O_4$ Double-Shell Heterostructures. Fifty milligrams of as-synthesized ZnO microspheres were dispersed into 47 mL of deionized water by ultrasonication, followed by addition of 3 mL of $FeSO_4$ solution (0.5 M). After constant stirring for 5 min, the resulting suspension was collected via centrifugation, washed with ethanol and deionized water several times, and dried at 60 °C. Finally, the precipitate was calcined at 550 °C for 3 h to obtain the ZnO/$ZnFe_2O_4$ double-shell heterostructure.

2.2. Characterization. X-ray powder diffraction (XRD) analysis was performed on a Rigaku D/max-2550 X-ray diffractometer with Cu Kα radiation (λ = 1.5406 Å), and the corresponding data was collected at 40 kV in the range of 20−80° (2θ). The surface morphology and microstructure of the products were observed using a JEOL JSM-7500F microscope, which was operated at 15 kV. Transmission electron microscopy (TEM) and high-resolution transmission electron microscopy (HRTEM) images were recorded on a JEOL JEM-2100F microscope with an accelerating voltage of 200 kV. The distribution of elements in crystal was characterized by an energy dispersive X-ray spectrometer (EDS) that was attached on TEM. The chemical composition was determined by using inductively coupled plasma (ICP) analysis that was characterized by a Perkin Elmer Optima 3300 DV ICP instrument. The specific surface areas of the obtained products were estimated based on the nitrogen adsorption−desorption isotherm, which was measured on a Gemini VII surface area and porosity system at 77 K. Pore diameter distribution was calculated by Barrett−Joyner−Halenda method using the desorption branch of the isotherms.

2.3. Fabrication and Measurement of Gas Sensors. Gas sensors based on the bare ZnO microspheres, pure $ZnFe_2O_4$ nanosheets, and ZnO/$ZnFe_2O_4$ composites were fabricated, and the detailed fabrication procedure of sensor devices was as follows: the as-synthesized sensing material was first mixed with deionized water to form a homogeneous paste and then coated onto a ceramic tube, at each end of which a pair of gold electrodes had been previously installed. In order to control the operating temperature of the sensor, a Ni−Cr alloy coil was inserted through the ceramic tube as a heater. After connecting the corresponding leads to the tube base, the sensor was finally constructed. The sensing properties of gas sensor were measured on a static system under laboratory conditions. Here, the response (S) of the sensor was defined as $S = R_a/R_g$, where R_a and R_g are the resistance value of gas sensors when exposed in air and in reducing gases. The response time and recovery time were defined as the time taken by the sensor to achieve 90% of the total resistance variation in the case of adsorption and desorption, respectively.

3. RESULTS AND DISCUSSION

3.1. Structural and Morphological Characteristics. The phase composition and purity of the as-synthesized products were characterized by powder X-ray diffraction (XRD). Figure 2 shows the typical XRD pattern of the as-synthesized hollow ZnO microspheres and ZnO/$ZnFe_2O_4$ composite. As can be seen, all of the diffraction peaks of ZnO sample (Figure 2a) matched well with those from standard wurtzite structured ZnO (JCPDS no. 36-1451). No other crystalline phase corresponding to impurity was detected, which indicated that the product had a high purity. For the composites, the diffraction peaks (Figure 2b) display a mixed crystal phases of ZnO and $ZnFe_2O_4$; besides the peaks being indexed to wurtzite structured ZnO with lattice parameters a = 3.249 Å and c = 5.206 Å, the residual peaks were in good agreement with those

DOI: 10.1021/acsami.5b04118
ACS Appl. Mater. Interfaces 2015, 7, 17811−17818

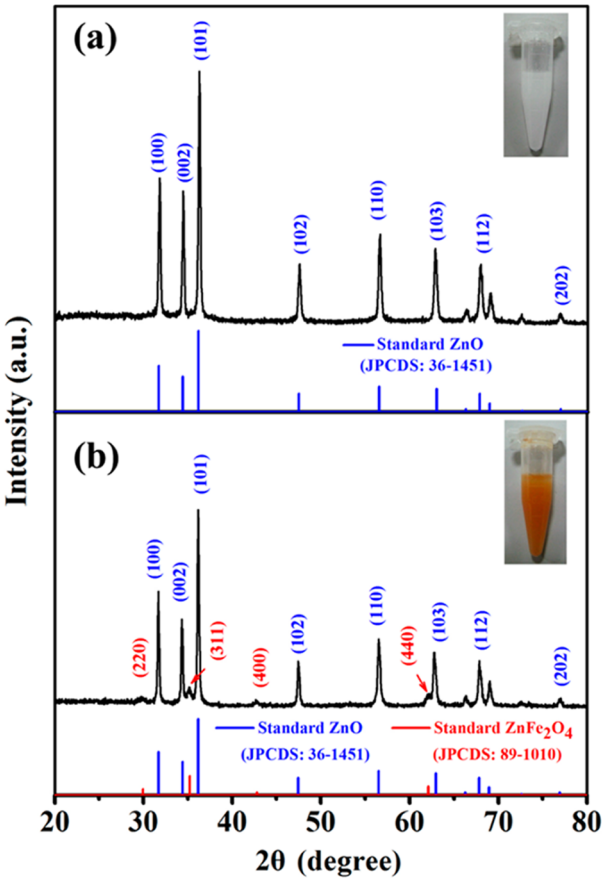

Figure 2. XRD patterns of as-prepared samples together with the standard diffraction patterns: (a) hollow ZnO microspheres, (b) ZnO/$ZnFe_2O_4$ composites.

from the standard card no. 89-1010, that is, could be indexed as cubic spinel $ZnFe_2O_4$ with lattice constants of a = 8.429 Å. By contrast, the peaks of $ZnFe_2O_4$ were weaker than those of ZnO in the composite, probably because of the large content of ZnO and/or the overlap of $ZnFe_2O_4$ and ZnO peaks. But obviously, it should be noted that the color of bare ZnO is very different from that of ZnO/$ZnFe_2O_4$, from which the decoration of pristine ZnO with $ZnFe_2O_4$ got confirmed (insets of Figure 2).

To further verify the composition of the outer shell of as-obtained sample, the ZnO core of ZnO/$ZnFe_2O_4$ composites was designed to be removed by etching the ZnO/$ZnFe_2O_4$ composites using ammonia solution, because of the fact that ZnO is soluble in ammonia solution. From the XRD pattern shown in Figure S1 (Supporting Information), it can be seen that all of the diffraction peaks could be indexed to $ZnFe_2O_4$ and that there was no diffraction peaks corresponding to ZnO left. Figure S2a and b display the SEM images of the $ZnFe_2O_4$ product, from which it can be found that the morphology of $ZnFe_2O_4$ still kept the sheetlike microstructure. The typical TEM image and the corresponding elemental mapping images of $ZnFe_2O_4$ nanosheets shown in Figure S3a–d indicate that the elements of Zn, Fe, and O were uniformly distributed within the $ZnFe_2O_4$ nanosheets. In addition, the EDS spectrum of Figure S3e also confirmed the coexistence of the above-mentioned three kinds of chemical elements. To accurately measure the chemical composition of these nanosheets, quantitative elemental analyses regarding the $ZnFe_2O_4$ nanosheets were measured by EDS (Table S1) and ICP (Table S2). As can be seen, both of the analysis results showed that the atomic ratio of Zn/Fe was about 1:2, which further confirmed the component of the outer shell being $ZnFe_2O_4$.

The detailed morphologies and microstructures of pristine ZnO were investigated by FESEM and TEM. As can be seen from Figure 3a, the as-prepared ZnO product exhibited uniform

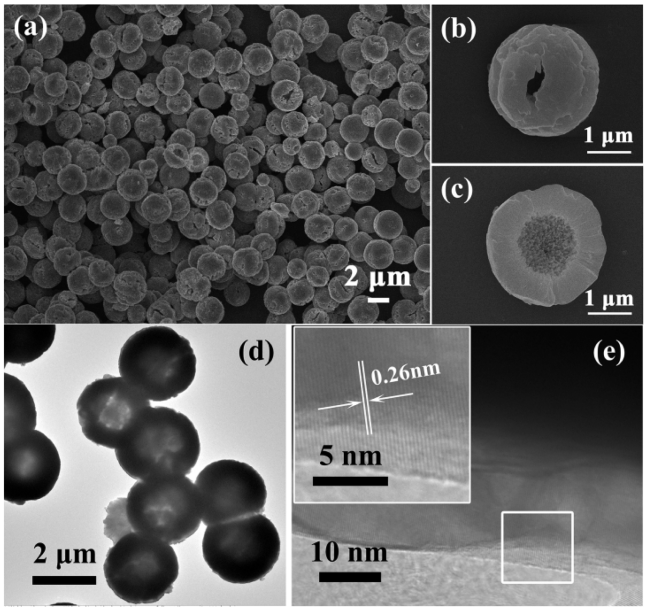

Figure 3. (a, b) Low- and high-magnification SEM images of bare ZnO; (c, d) cross-sectional SEM view and TEM image of hollow ZnO microspheres; (e) HRTEM image of ZnO crystal attached on the surface of bare ZnO.

size with spherical architectures. The high-magnification FESEM images (Figure 3b) indicated that these pristine ZnO microspheres had a clean surface and their average diameter was about 2.5 μm. Figure 3c presents the cross section of a single ZnO microsphere, from which the internal hollow architecture could be clearly identified and the inner diameter was observed to be ~1 μm. To get more detailed structural information on such microspheres, the TEM and HRTEM observations were carried out. As can be seen from the typical TEM image (Figure 3d), the hollow nature of these ZnO microspheres got further confirmed by the different contrast between the light center and the dark fringe. Figure 3e and its inset are the HRTEM images taken from the surface of spherical shell, and it can be seen that the obtained ZnO was highly crystallized and the marked interplanar spacing between the adjacent lattice fringes was 0.26 nm, which can be readily indexed to the {0002} planes of the wurtzite ZnO.

Considering that gas sensing is a surface-related phenomenon, the dense and clean surface of pure ZnO microspheres cannot provide enough active sites for gas adsorption and sensing reaction. Thus, we did some modification to these pristine ZnO microspheres. After immersing these pristine ZnO microspheres into $FeSO_4$ solution for only 5 min at ambient temperature, a thin layer of $ZnFe_2O_4$ nanosheets uniformly grew on the surface of ZnO hollow spheres. As can be seen from Figure 4a, the as-synthesized ZnO/$ZnFe_2O_4$ heterostructures were well-dispersed and kept the initial spherical architecture. The enlarged SEM image (Figure 4b) reveals that many randomly arranged nanosheets were attached on the surface of ZnO microspheres, resulting in a more porous and

DOI: 10.1021/acsami.5b04118
ACS Appl. Mater. Interfaces 2015, 7, 17811–17818

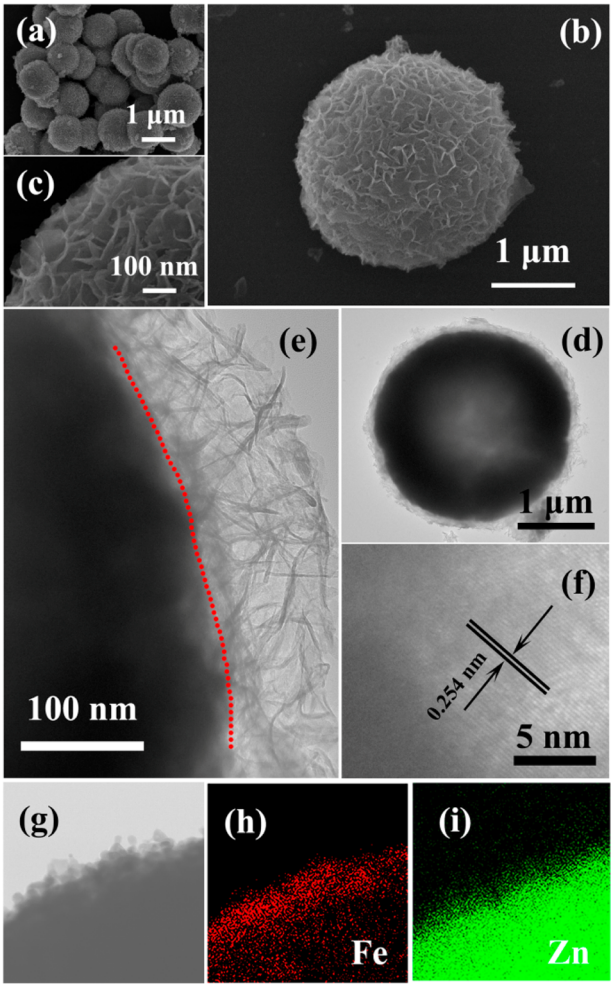

Figure 4. Structural characterizations of $ZnFe_2O_4$-decorated ZnO heterostructures: (a–c) SEM images at different magnification, (d, e) TEM images, (f) HRTEM image, (g) scanning TEM image, and (h, i) elemental mapping images.

complex surface. Figure 4c clearly displays the structure of the obtained 2D $ZnFe_2O_4$ nanosheets. It can be seen that these nanosheets were ultrathin and the average thickness of nanosheets was about 10 nm. When characterized using transmission electron microscope (Figure 4d), a distinctive bilayer structure consisting of a hollow ZnO core and thin $ZnFe_2O_4$ shell could be easily identified. The high-magnification TEM image (Figure 4e) confirmed that $ZnFe_2O_4$ nanosheets merged well with ZnO core and the thickness of $ZnFe_2O_4$ shell was about 100 nm. Figure 4f presents a HRTEM image of $ZnFe_2O_4$ nanosheets located on the surface. The lattice spacing was measured to be 0.254 nm, which was consistent with the distance between the {311} planes of the cubic $ZnFe_2O_4$. To further identify the spatial distribution of Fe and Zn in the ZnO/$ZnFe_2O_4$ heterostructure (shown in Figure 4g), the corresponding elemental mappings were recorded in Figure 4h and i. It can be seen that the signals of Fe were mainly detected in the shell region and seldom in the core region. On the contrary, for Zn element, most of signals concentrated in the core region, and a few of them came from the shell region.

Since the porous characteristics of the as-synthesized samples has important influence on the gas-sensing performance, the BET surface area and pore-size distribution were investigated based on nitrogen adsorption–desorption isotherms, as shown in Figure 5. The BET surface areas of hollow ZnO and ZnO/$ZnFe_2O_4$ core–shell structure were calculated to be 13.7 and 53.8 $m^2\ g^{-1}$, respectively. The pore size of the obtained samples were mainly distributed around about 60–90 nm. On the basis of above results, it is obvious that ZnO/$ZnFe_2O_4$ heterostructure has much larger surface area than the pristine ZnO microspheres, which directly confirmed the significance of designing and synthesizing such novel heterostructure.

3.2. Gas-Sensing Characteristics. To demonstrate these novel ZnO/$ZnFe_2O_4$ composites might bring about more excellent sensing properties, gas sensors based on the as-prepared ZnO/$ZnFe_2O_4$, ZnO hollow spheres and $ZnFe_2O_4$ nanosheets were fabricated and their gas sensing properties were investigated (Details about the preparation $ZnFe_2O_4$ nanosheets are presented in the Supporting Information). Operating temperature is one of the most important criterions for a successful gas sensor. Many processes associated with gas sensing, such as adsorption/desorption of gases and surface reactions, are subject to the operating temperature. Therefore, we have to start the various sensing tests from the temperature-dependent behavior. Figure 6a displays the response of the sensors to 100 ppm acetone as a function of operating

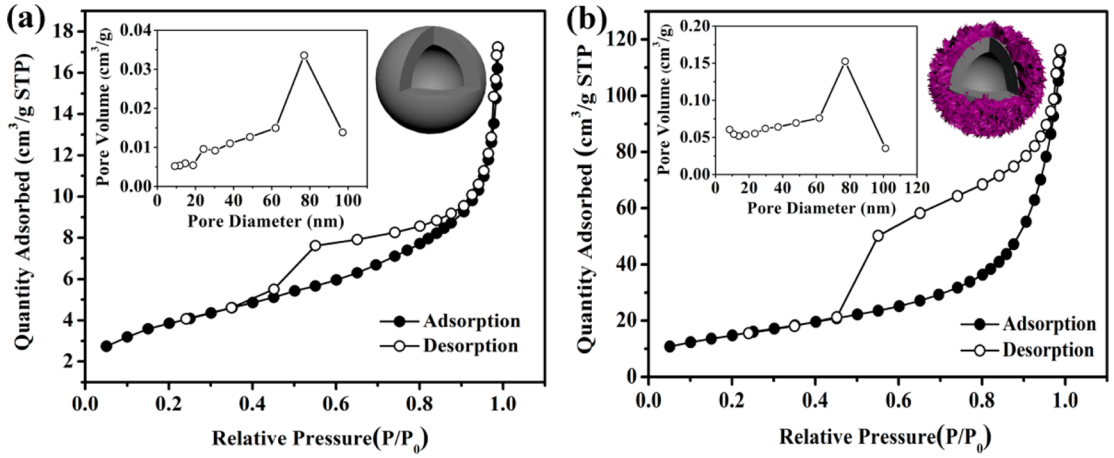

Figure 5. Nitrogen adsorption/desorption isotherms and pore size distribution of as-obtained products: (a) ZnO microspheres; (b) ZnO/$ZnFe_2O_4$ heterostructures.

DOI: 10.1021/acsami.5b04118
ACS Appl. Mater. Interfaces 2015, 7, 17811–17818

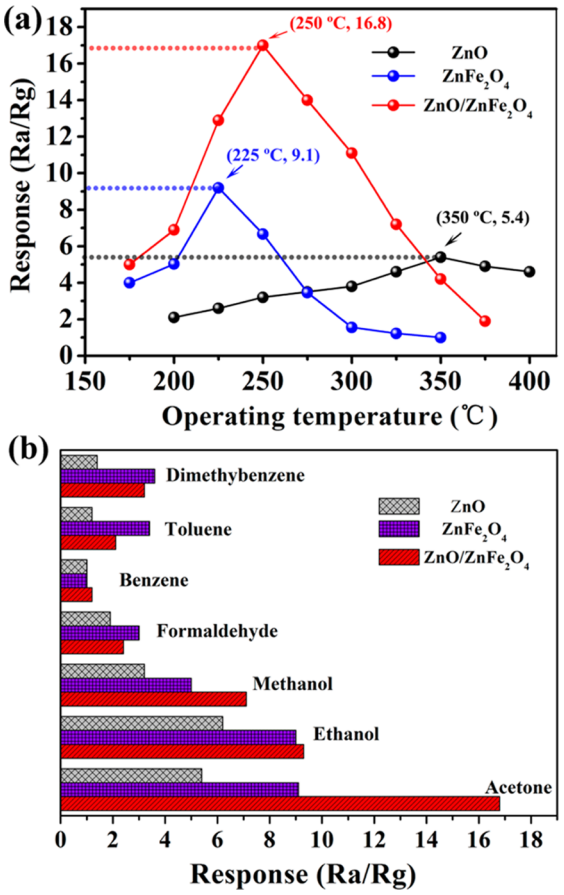

Figure 6. (a) Temperature-dependent gas-sensing responses of ZnO hollow microspheres, $ZnFe_2O_4$ nanosheets, and $ZnO/ZnFe_2O_4$ composites. (b) Selectivities of three kinds of sensors upon exposure to 100 ppm of various interfering gases at their optimum operating temperature.

temperature. As can be seen from the results, with the increase of operating temperature, all of the tested sensors showed an "increase−maximum−decrease" pattern. Generally speaking, if the temperature imposed on gas sensor was low, the reaction between tested gas molecules and surface adsorbed oxygen species was too inert to give a high response. As the operating temperature increased, the overall reaction was accelerated and thus led to a significant enhancement of response. However, compared with the rapid reaction on the surface of sensing materials, the diffusion of tested gases became limited at much higher temperature. Once the tested gases diffused to the material surface, they would be reduced/oxidized rapidly without affecting the electrical conductivity of the sensing layer. As a result, the response of the sensor became low again.[4,40] For the sensor based on hollow ZnO microspheres, the maximum response appearing at its optimum operating temperature (350 °C) was 5.4. For the sensor based on $ZnFe_2O_4$ nanosheets, the maximum response to 100 ppm acetone was 9.1, which was obtained at 225 °C. When the working temperature was 250 °C, the sensor based on $ZnO/ZnFe_2O_4$ composites reached its maximum response of 16.8. By contrast, it is noteworthy that the optimum operating temperature of the sensor based on $ZnFe_2O_4$ and $ZnO/ZnFe_2O_4$ composites was much lower than that of the sensor based on pure ZnO. Notably, though the optimum operating temperature of $ZnO/ZnFe_2O_4$ composites was slightly higher than that of $ZnFe_2O_4$ nanosheets, the $ZnO/ZnFe_2O_4$ heterostructure exhibited about 1.8 and 3 times enhancement in gas response to 100 ppm acetone in comparison to $ZnFe_2O_4$ nanosheets and ZnO hollow microspheres, respectively.

As another important criterion of gas sensors, the selectivities of the three kinds of sensors were investigated by comparing the responses to a variety of volatile organic compound gases, such as acetone, ethanol, methanol, formaldehyde, benzene, toluene, and dimethylbenzene. As can be seen from Figure 6b, the responses of pristine ZnO hollow microspheres and $ZnFe_2O_4$ nanosheets toward acetone were relatively low and quite similar to the other interfering gases, which make the selective detection of acetone difficult when working at the optimum operating temperature. In stark contrast to the pristine ZnO or pure $ZnFe_2O_4$, the sensor based on $ZnO/ZnFe_2O_4$ composites showed much higher response toward acetone in comparison to other tested gases. From this perspective, the present sensor based on $ZnO/ZnFe_2O_4$ composites can be a better candidate for the selective detection of acetone gas.

In addition, further analyses regarding to the three gas sensors versus different concentrations of acetone were carried out, and the results are presented in Figure 7a. As can be seen, the responses of the gas sensors gradually increased as the acetone concentration increased from 5 to 700 ppm. Given that

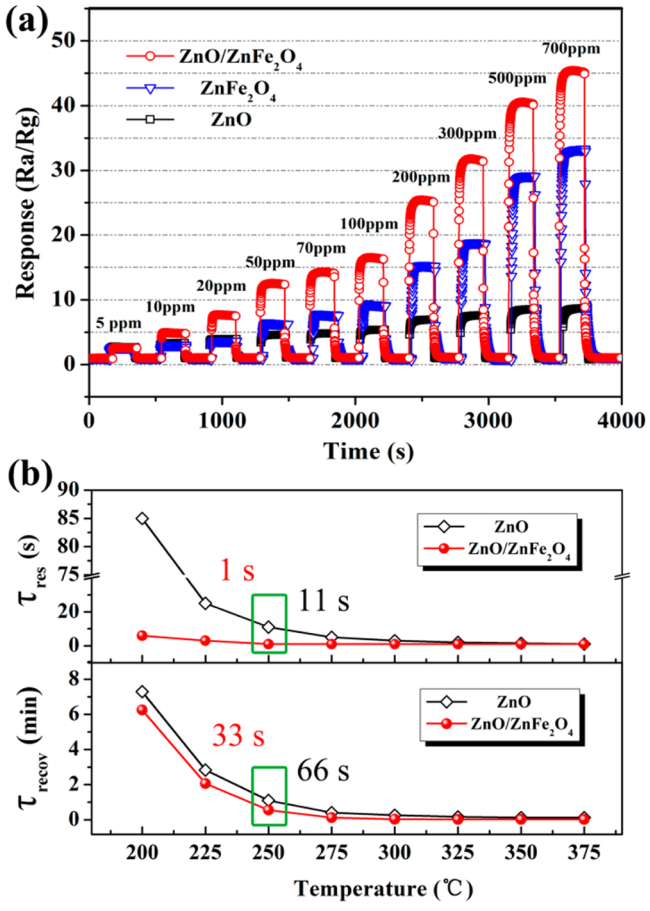

Figure 7. (a) Gas responses of the sensors based on bare ZnO, pure $ZnFe_2O_4$, and $ZnO/ZnFe_2O_4$ composites as a function of acetone concentration from 5 to 700 ppm. (b) Response and recover times versus operating temperature of pristine ZnO microspheres and $ZnFe_2O_4$-decorated ZnO heterostructures.

DOI: 10.1021/acsami.5b04118
ACS Appl. Mater. Interfaces 2015, 7, 17811−17818

the value of response ($R_a/R_g > 2$) was usually chosen as the criterion for a valid response,[41] it is thus expected that the three gas sensors based on bare ZnO, pure $ZnFe_2O_4$, and ZnO/$ZnFe_2O_4$ composites were capable of detecting acetone concentration as low as 5 ppm. Moreover, it is worth noting that the response of the sensor based on ZnO/$ZnFe_2O_4$ composites displayed a much faster growth rate and quite improved response compared to its two counterparts. Evidently, simply by some modifications on the surface of bare ZnO, the gas-sensing performance toward acetone can be effectively improved. Moreover, to shed light on whether the different molar ratios of $ZnFe_2O_4$ to ZnO will have an influence on the sensing properties, two other ZnO/$ZnFe_2O_4$ composites were synthesized (Table S3 and Figure S4) and investigated as acetone gas sensors. Figure S5a presents the sensors based on as-synthesized pure ZnO and ZnO/$ZnFe_2O_4$ composites to 100 ppm acetone at different operating temperature. It can be observed that the gas-sensing performances were all improved after the decoration with $ZnFe_2O_4$ nanosheets. However, due to the differences in coverage of $ZnFe_2O_4$, the gas responses between these ZnO/$ZnFe_2O_4$ composites were a little different. In addition, when the sensors were working at the optimal operating temperature, the sensor based on S2 exhibited the highest responses under different acetone concentration, as shown in Figure S5b. Thus, the sensing material S2 was selected as the optimal ZnO/$ZnFe_2O_4$ heterostructure in this work.

As mentioned previously, the increase of operating temperature can facilitate and accelerate the gas-sensing reaction; thus, the rates of response/recover at different operating temperature were also investigated (Figure 7b). Obviously, the response/recover times were temperature-dependent and markedly reduced with the increase of temperature. In comparison to the pristine ZnO hollow microspheres, the sensors using as-prepared ZnO/$ZnFe_2O_4$ composites exhibited a faster response and recover characteristics. For example, when the sensor based on ZnO/$ZnFe_2O_4$ composites worked at optimum operating temperature (250 °C), the response and recover time were only 1 and 33 s respectively, while the response and recover times taken by the sensor based on pristine ZnO were as long as 11 and 66 s at the same temperature. From the view of practical application, the fast response/recover behaviors make ZnO/$ZnFe_2O_4$ composites more suitable for gas detection. Furthermore, their response/recover behavior could be well repeated, and there is no clear attenuation in response upon alternately exposed to air and 100 ppm acetone gas for several cycles. This quite similar transients observed here indicated the good repeatability and stability of the as-fabricated sensor (Figure 8).

3.3. Gas-Sensing Mechanism. It is well-known that gas sensing is a surface-related phenomenon, and up to now, the most popular and widely accepted sensing principle is based on the change of sensor resistance arising from the adsorption/desorption of gaseous molecules and the interaction among these absorbed gas molecules on the surface of sensing film.[40,42] For the sensors based on bare ZnO hollow spheres, upon exposure to air, oxygen molecules would be adsorbed on the inner/outer surface of the ZnO and ionized to the chemisorbed oxygen species (O^{2-}, O^-, or O_2^-) by capturing free electrons from the conduction band of ZnO. As a result, along with the formation of electron depletion layers on the surface domains of ZnO, the conductivity of the sensor was also decreased. If reducing gas like acetone was introduced at this moment, these

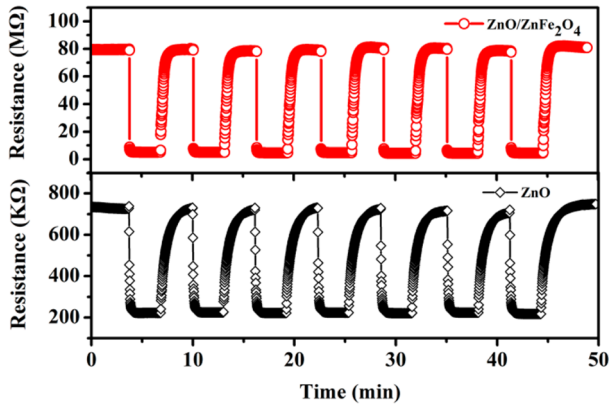

Figure 8. Dynamical response transients of ZnO/$ZnFe_2O_4$ composites and ZnO hollow spheres to 100 ppm acetone at 250 °C.

gas molecules would react with adsorbed oxygen species, eq 1, and the electrons trapped by the oxygen adsorbates were reinjected into the conduction band, which eventually led to a remarkable decrease of the resistance.

$$CH_3COCH_3 + 8O^- \leftrightarrow 3CO_2 + 3H_2O + 8e^- \quad (1)$$

For $ZnFe_2O_4$-decorated ZnO hybrid composite, in virtue of its unique structural characteristics, the present ZnO/$ZnFe_2O_4$ composites exhibit much larger special surface area in comparison to the bare ZnO hollow microspheres (Figure 5). Therefore, by contrast, ZnO/$ZnFe_2O_4$ composites possess more reaction sites and the quantity of absorbed oxygen species on the surface was increased, which finally led to a high sensitivity. Furthermore, the well-aligned $ZnFe_2O_4$ nanosheets on the outsides endow ZnO/$ZnFe_2O_4$ composites a porous surface, which can significantly facilitate the diffusion of the oxygen and test gases toward active sites. As a consequence, faster response and recover transients of ZnO/$ZnFe_2O_4$ composites were obtained. Meanwhile, the heterojunctions between $ZnFe_2O_4$ nanosheets and ZnO microspheres also contributed a lot to the enhanced performance. According to the theory of semiconductor physics, when two different metal oxides contact each other, carrier depletion layers will emerge near the interfaces. Hence, the barrier height of ZnO/$ZnFe_2O_4$ composites increased significantly, which eventually resulted in an obvious increase in the sensor resistance (as shown in Figure 8). Because the definition of response was depicted as the ratio of R_a/R_g, the high value of initial resistance is beneficial to increasing the response of gas sensor.[43] As a result, the sensor based on ZnO/$ZnFe_2O_4$ heterostructure showed better sensing performance compared with the bare ZnO microspheres.

4. CONCLUSIONS

In conclusion, ZnO/$ZnFe_2O_4$ microstructures with a distinctive double−shell configuration have been successfully prepared by a mild two-step method, which involved the microwave-assisted synthesis of ZnO hollow microspheres and subsequent modification with $ZnFe_2O_4$ nanosheets at room temperature. The present method is believed to be applicable to synthesize other ZnO/$ZnFe_2O_4$ heterostructures with various morphologies. When tested as a potential sensing material for gas sensing, the as-prepared ZnO/$ZnFe_2O_4$ composites exhibited a remarkable enhancement compared to the individual ZnO and $ZnFe_2O_4$ components in many aspects, such as sensitivity, operating temperature, and response/recover behavior. The

DOI: 10.1021/acsami.5b04118
ACS Appl. Mater. Interfaces 2015, 7, 17811−17818

enhanced sensing performances of $ZnFe_2O_4$-decorated ZnO were most likely ascribed to three factors. First, the quantity of reaction sites and absorbed oxygen species on the surface was obviously increased owing to the large special surface area of $ZnO/ZnFe_2O_4$ composites. Second, the gases diffusion rate was considerably enhanced with the assistance of the porous $ZnFe_2O_4$ layer. Third, the initial resistance of $ZnO/ZnFe_2O_4$ was significantly increased along with the formation of heterojunction between the two metal oxides.

■ ASSOCIATED CONTENT

Supporting Information

The Supporting Information is available free of charge on the ACS Publications website at DOI: 10.1021/acsami.5b04118.

Synthesis of $ZnFe_2O_4$ nanosheets; XRD pattern and SEM images of $ZnFe_2O_4$ nanosheets; TEM image and corresponding elemental mapping images of $ZnFe_2O_4$ nanosheets; SEM images of as-obtained $ZnO/ZnFe_2O_4$ heterostructures; relationship of responses versus operating temperature; response of the sensors to different concentrations of acetone at their optimum operating temperature; elemental analysis reports of EDS; inductively coupled plasma (ICP) analysis of $ZnFe_2O_4$ nanosheets; experimental parameters for the synthesis of $ZnO/ZnFe_2O_4$ heterostructures (PDF)

■ AUTHOR INFORMATION

Corresponding Authors

*E-mail: spmaster2008@163.com.
*E-mail: lugy@jlu.edu.cn. Fax: +86 431 85167808. Tel.: +86 431 85167808.

Author Contributions

The manuscript was written through contributions of all authors. All authors have given approval to the final version of the manuscript.

Notes

The authors declare no competing financial interest.

■ ACKNOWLEDGMENTS

This work is supported by the National Nature Science Foundation of China (Nos. 61374218, 61134010, and 61327804), Program for Chang Jiang Scholars and Innovative Research Team in University (No. IRT13018), National High-Tech Research and Development Program of China (863 Program, Nos. 2013AA030902 and 2014AA06A505), and Project 2015094 Supported by Graduate Innovation Fund of Jilin University.

■ ABBREVIATIONS

ZHS, ZnO hollow microspheres
MOS, metal oxide semiconductors
VOC, volatile organic compounds
XRD, X-ray powder diffraction
FESEM, field emission scanning electron microscopy
TEM, transmission electron microscopy
HRTEM, high-resolution transmission electron microscopy
EDS, energy dispersive X-ray spectrometer
ICP, inductively coupled plasma

■ REFERENCES

(1) Franke, M. E.; Koplin, T. J.; Simon, U. Metal and Metal Oxide Nanoparticles in Chemiresistors: Does the Nanoscale Matter? *Small* **2006**, *2*, 36−50.
(2) Kim, H.-R.; Haensch, A.; Kim, I.-D.; Barsan, N.; Weimar, U.; Lee, J.-H. The Role of NiO Doping in Reducing the Impact of Humidity on the Performance of SnO_2-Based Gas Sensors: Synthesis Strategies, and Phenomenological and Spectroscopic Studies. *Adv. Funct. Mater.* **2011**, *21*, 4456−4463.
(3) Du, N.; Zhang, H.; Chen, B. D.; Ma, X. Y.; Liu, Z. H.; Wu, J. B.; Yang, D. R. Porous Indium Oxide Nanotubes: Layer-by-Layer Assembly on Carbon-Nanotube Templates and Application for Room-Temperature NH_3 Gas Sensors. *Adv. Mater.* **2007**, *19*, 1641−1645.
(4) Li, X.; Zhou, X.; Guo, H.; Wang, C.; Liu, J.; Sun, P.; Liu, F.; Lu, G. Design of Au@ZnO Yolk-Shell Nanospheres with Enhanced Gas Sensing Properties. *ACS Appl. Mater. Interfaces* **2014**, *6*, 18661−18667.
(5) Sun, P.; Liu, Y.; Li, X.; Sun, Y.; Liang, X.; Liu, F.; Lu, G. Facile Synthesis and Gas-Sensing Properties of Monodisperse α-Fe_2O_3 Discoid Crystals. *RSC Adv.* **2012**, *2*, 9824−9829.
(6) Li, X. L.; Lou, T. J.; Sun, X. M.; Li, Y. D. Highly Sensitive WO_3 Hollow-Sphere Gas Sensors. *Inorg. Chem.* **2004**, *43*, 5442−5449.
(7) Cho, N. G.; Woo, H. S.; Lee, J. H.; Kim, I. D. Thin-Walled NiO Tubes Functionalized with Catalytic Pt for Highly Selective C_2H_5OH Sensors Using Electrospun Fibers as a Sacrificial Template. *Chem. Commun.* **2011**, *47*, 11300−11302.
(8) Sun, C.; Rajasekhara, S.; Chen, Y.; Goodenough, J. B. Facile Synthesis of Monodisperse Porous Co_3O_4 Microspheres with Superior Ethanol Sensing Properties. *Chem. Commun.* **2011**, *47*, 12852−12854.
(9) Kim, Y.-S.; Hwang, I.-S.; Kim, S.-J.; Lee, C.-Y.; Lee, J.-H. CuO Nanowire Gas Sensors for Air Quality Control in Automotive Cabin. *Sens. Actuators, B* **2008**, *135*, 298−303.
(10) Wang, Z.; Xiao, Y.; Cui, X.; Cheng, P.; Wang, B.; Gao, Y.; Li, X.; Yang, T.; Zhang, T.; Lu, G. Humidity Sensing Properties of Urchin-Like CuO Nanostructures Modified by Reduced Graphene Oxide. *ACS Appl. Mater. Interfaces* **2014**, *6*, 3888−3895.
(11) Cai, Y.; Li, X.; Liu, Y.; Du, S.; Cheng, P.; Liu, F.; Shimanoe, K.; Yamazoe, N.; Lu, G. Hollow Cylinder ZnO/SnO_2 Nanostructures Synthesized by Ultrasonic Spray Pyrolysis and Their Gas-Sensing Performance. *CrystEngComm* **2014**, *16*, 6135−6140.
(12) Wang, L.; Deng, J.; Lou, Z.; Zhang, T. Cross-Linked P-Type Co_3O_4 Octahedron Nanoparticles in 1 D N-Type TiO_2 Nanofibers for High-Performance Sensing Devices. *J. Mater. Chem. A* **2014**, *2*, 10022−10028.
(13) Bao, M.; Chen, Y.; Li, F.; Ma, J.; Lv, T.; Tang, Y.; Chen, L.; Xu, Z.; Wang, T. Plate-Like P−N Heterogeneous NiO/WO_3 Nanocomposites for High Performance Room Temperature NO_2 Sensors. *Nanoscale* **2014**, *6*, 4063−4066.
(14) Sun, P.; Zhou, X.; Wang, C.; Shimanoe, K.; Lu, G.; Yamazoe, N. Hollow SnO_2/α-Fe_2O_3 Spheres with Double-Shell Structure for Gas Sensor. *J. Mater. Chem. A* **2014**, *2*, 1302−1308.
(15) Kim, S.-J.; Na, C. W.; Hwang, I.-S.; Lee, J.-H. One-Pot Hydrothermal Synthesis of CuO−ZnO Composite Hollow Spheres for Selective H_2S Detection. *Sens. Actuators, B* **2012**, *168*, 83−89.
(16) Hjiri, M.; El Mir, L.; Leonardi, S. G.; Pistone, A.; Mavilia, L.; Neri, G. Al-Doped ZnO for Highly Sensitive CO Gas Sensors. *Sens. Actuators, B* **2014**, *196*, 413−420.
(17) Law, J. B.; Thong, J. T. Improving the NH_3 Gas Sensitivity of ZnO Nanowire Sensors by Reducing the Carrier Concentration. *Nanotechnology* **2008**, *19*, 205502.
(18) Anantachaisilp, S.; Smith, S. M.; Ton-That, C.; Osotchan, T.; Moon, A. R.; Phillips, M. R. Tailoring Deep Level Surface Defects in ZnO Nanorods for High Sensitivity Ammonia Gas Sensing. *J. Phys. Chem. C* **2014**, *118*, 27150−27156.
(19) Spencer, M. J. S.; Yarovsky, I. ZnO Nanostructures for Gas Sensing: Interaction of NO_2, NO, O, and N with the ZnO $(10\bar{1}0)$ Surface. *J. Phys. Chem. C* **2010**, *114*, 10881−10893.

DOI: 10.1021/acsami.5b04118
ACS Appl. Mater. Interfaces 2015, 7, 17811−17818

(20) Rai, P.; Kwak, W. K.; Yu, Y. T. Solvothermal Synthesis of ZnO Nanostructures and Their Morphology-Dependent Gas-Sensing Properties. *ACS Appl. Mater. Interfaces* **2013**, *5*, 3026−3032.
(21) Bai, S.; Liu, X.; Li, D.; Chen, S.; Luo, R.; Chen, A. Synthesis of ZnO Nanorods and Its Application in NO_2 Sensors. *Sens. Actuators, B* **2011**, *153*, 110−116.
(22) Jing, Z.; Zhan, J. Fabrication and Gas-Sensing Properties of Porous ZnO Nanoplates. *Adv. Mater.* **2008**, *20*, 4547−4551.
(23) Li, X. W.; Sun, P.; Yang, T. L.; Zhao, J.; Wang, Z. Y.; Wang, W. N.; Liu, Y. P.; Lu, G. Y.; Du, Y. Template-Free Microwave-Assisted Synthesis of ZnO Hollow Microspheres and Their Application in Gas Sensing. *CrystEngComm* **2013**, *15*, 2949−2955.
(24) Woo, H. S.; Kwak, C. H.; Chung, J. H.; Lee, J. H. Co-Doped Branched ZnO Nanowires for Ultraselective and Sensitive Detection of Xylene. *ACS Appl. Mater. Interfaces* **2014**, *6*, 22553−22560.
(25) Zhou, X.; Liu, J.; Wang, C.; Sun, P.; Hu, X.; Li, X.; Shimanoe, K.; Yamazoe, N.; Lu, G. Highly Sensitive Acetone Gas Sensor Based on Porous $ZnFe_2O_4$ Nanospheres. *Sens. Actuators, B* **2015**, *206*, 577−583.
(26) Sutka, A.; Zavickis, J.; Mezinskis, G.; Jakovlevs, D.; Barloti, J. Ethanol Monitoring by $ZnFe_2O_4$ Thin Film Obtained by Spray Pyrolysis. *Sens. Actuators, B* **2013**, *176*, 330−334.
(27) Yao, C.; Zeng, Q.; Goya, G. F.; Torres, T.; Liu, J.; Wu, H.; Ge, M.; Zeng, Y.; Wang, Y.; Jiang, J. Z. $ZnFe_2O_4$ Nanocrystals: Synthesis and Magnetic Properties. *J. Phys. Chem. C* **2007**, *111*, 12274−12278.
(28) Pereira, C.; Pereira, A. M.; Fernandes, C.; Rocha, M.; Mendes, R.; Fernández-García, M. P.; Guedes, A.; Tavares, P. B.; Grenèche, J.-M.; Araújo, J. o. P.; Freire, C. Superparamagnetic MFe_2O_4 (M = Fe, Co, Mn) Nanoparticles: Tuning the Particle Size and Magnetic Properties through a Novel One-Step Coprecipitation Route. *Chem. Mater.* **2012**, *24*, 1496−1504.
(29) Kumbhar, S. S.; Mahadik, M. A.; Shinde, S. S.; Rajpure, K. Y.; Bhosale, C. H. Fabrication of $ZnFe_2O_4$ Films and Its Application in Photoelectrocatalytic Degradation of Salicylic Acid. *J. Photochem. Photobiol., B* **2015**, *142*, 118−123.
(30) Dom, R.; Subasri, R.; Hebalkar, N. Y.; Chary, A. S.; Borse, P. H. Synthesis of a Hydrogen Producing Nanocrystalline $ZnFe_2O_4$ Visible Light Photocatalyst Using a Rapid Microwave Irradiation Method. *RSC Adv.* **2012**, *2*, 12782−12791.
(31) Cherian, C. T.; Sundaramurthy, J.; Reddy, M. V.; Suresh Kumar, P.; Mani, K.; Pliszka, D.; Sow, C. H.; Ramakrishna, S.; Chowdari, B. V. Morphologically Robust $NiFe_2O_4$ Nanofibers as High Capacity Li-Ion Battery Anode Material. *ACS Appl. Mater. Interfaces* **2013**, *5*, 9957−9963.
(32) Bresser, D.; Paillard, E.; Kloepsch, R.; Krueger, S.; Fiedler, M.; Schmitz, R.; Baither, D.; Winter, M.; Passerini, S. Carbon Coated $ZnFe_2O_4$ Nanoparticles for Advanced Lithium-Ion Anodes. *Adv. Energy Mater.* **2013**, *3*, 513−523.
(33) Won, J. M.; Choi, S. H.; Hong, Y. J.; Ko, Y. N.; Kang, Y. C. Electrochemical Properties of Yolk-Shell Structured $ZnFe_2O_4$ Powders Prepared by a Simple Spray Drying Process as Anode Material for Lithium-Ion Battery. *Sci. Rep.* **2014**, *4*, 5857.
(34) Cao, J.; Xing, J.; Zhang, Y.; Tong, H.; Bi, Y.; Kako, T.; Takeguchi, M.; Ye, J. Photoelectrochemical Properties of Nano-multiple $CaFe_2O_4/ZnFe_2O_4$ PN Junction Photoelectrodes. *Langmuir* **2013**, *29*, 3116−3124.
(35) Karpova, S.; Moshnikov, V.; Mjakin, S.; Kolovangina, E. Surface Functional Composition and Sensor Properties of ZnO, Fe_2O_3, and $ZnFe_2O_4$. *Semiconductors* **2013**, *47*, 392−395.
(36) Woo, H. S.; Na, C. W.; Kim, I. D.; Lee, J. H. Highly Sensitive and Selective Trimethylamine Sensor Using One-Dimensional ZnO-Cr_2O_3 Hetero-Nanostructures. *Nanotechnology* **2012**, *23*, 245501.
(37) Schileo, G. Recent Developments in Ceramic Multiferroic Composites Based on Core/Shell and Other Heterostructures Obtained by Sol−Gel Routes. *Prog. Solid State Chem.* **2013**, *41*, 87−98.
(38) Wang, W. W.; Zhu, Y. J.; Yang, L. X. ZnO−SnO_2 Hollow Spheres and Hierarchical Nanosheets: Hydrothermal Preparation, Formation Mechanism, and Photocatalytic Properties. *Adv. Funct. Mater.* **2007**, *17*, 59−64.
(39) Anandan, S.; Wu, J. J. Ultrasound Assisted Synthesis of TiO_2-WO_3 Heterostructures for the Catalytic Degradation of Tergitol (NP-9) in Water. *Ultrason. Sonochem.* **2014**, *21*, 1284−1288.
(40) Batra, A. K.; Chilvery, A. K.; Guggilla, P.; Aggarwal, M.; Currie, J. R. Micro- and Nano-Structured Metal Oxides Based Chemical Sensors: An Overview. *J. Nanosci. Nanotechnol.* **2014**, *14*, 2065−2085.
(41) Cho, Y. H.; Liang, X.; Kang, Y. C.; Lee, J.-H. Ultrasensitive Detection of Trimethylamine Using Rh-Doped SnO_2 Hollow Spheres Prepared by Ultrasonic Spray Pyrolysis. *Sens. Actuators, B* **2015**, *207*, 330−337.
(42) Yamazoe, N.; Shimanoe, K. New Perspectives of Gas Sensor Technology. *Sens. Actuators, B* **2009**, *138*, 100−107.
(43) Miller, D. R.; Akbar, S. A.; Morris, P. A. Nanoscale Metal Oxide-Based Heterojunctions for Gas Sensing: A Review. *Sens. Actuators, B* **2014**, *204*, 250−272.

DOI: 10.1021/acsami.5b04118
ACS Appl. Mater. Interfaces 2015, 7, 17811−17818